Accepted Manuscript

Title: [Ni(2,2′-bipy)$_3$]Cl2 activated sepiolite clay with high photocatalytic and oil–water separation abilities

Authors: Shunqiang Chen, Wenliang Li, Feng Li, Taohai Li, Wei Cao

PII: S1226-086X(18)30680-4
DOI: https://doi.org/10.1016/j.jiec.2019.07.028
Reference: JIEC 4670

To appear in:

Received date: 15 September 2018
Revised date: 27 March 2019
Accepted date: 13 July 2019

Please cite this article as: Chen S, Li W, Li F, Li T, Cao W, [Ni(2,2′-bipy)$_3$]Cl2 activated sepiolite clay with high photocatalytic and oil–water separation abilities, *Journal of Industrial and Engineering Chemistry* (2019), https://doi.org/10.1016/j.jiec.2019.07.028

This is a PDF file of an unedited manuscript that has been accepted for publication. As a service to our customers we are providing this early version of the manuscript. The manuscript will undergo copyediting, typesetting, and review of the resulting proof before it is published in its final form. Please note that during the production process errors may be discovered which could affect the content, and all legal disclaimers that apply to the journal pertain.

ACCEPTED MANUSCRIPT

$[Ni(2,2'\text{-bipy})_3]Cl_2$ activated sepiolite clay with high photocatalytic and oil–water separation abilities

Shunqiang Chen[a], Wenliang Li[a], Feng Li[a,*], Taohai Li[a,*], Wei Cao[b]

[a]*College of Chemistry, Key Lab of Environment Friendly Chemistry and Application in Ministry of Education, Xiangtan University, Xiangtan, 411105, China.*

[b]*Nano and Molecular Materials Research Unit, Faculty of Science, University of Oulu, P.O. Box 3000, FIN-90014, Finland*

[*]Corresponding Author: Tel.: +86-731-58292202; fax: +86-731-8292251;

E-mail address: fengli_xtu@hotmail.com (F. Li) hnlth@xtu.edu.cn (T. Li)

Graphical abstract

ACCEPTED MANUSCRIPT

ACCEPTED MANUSCRIPT

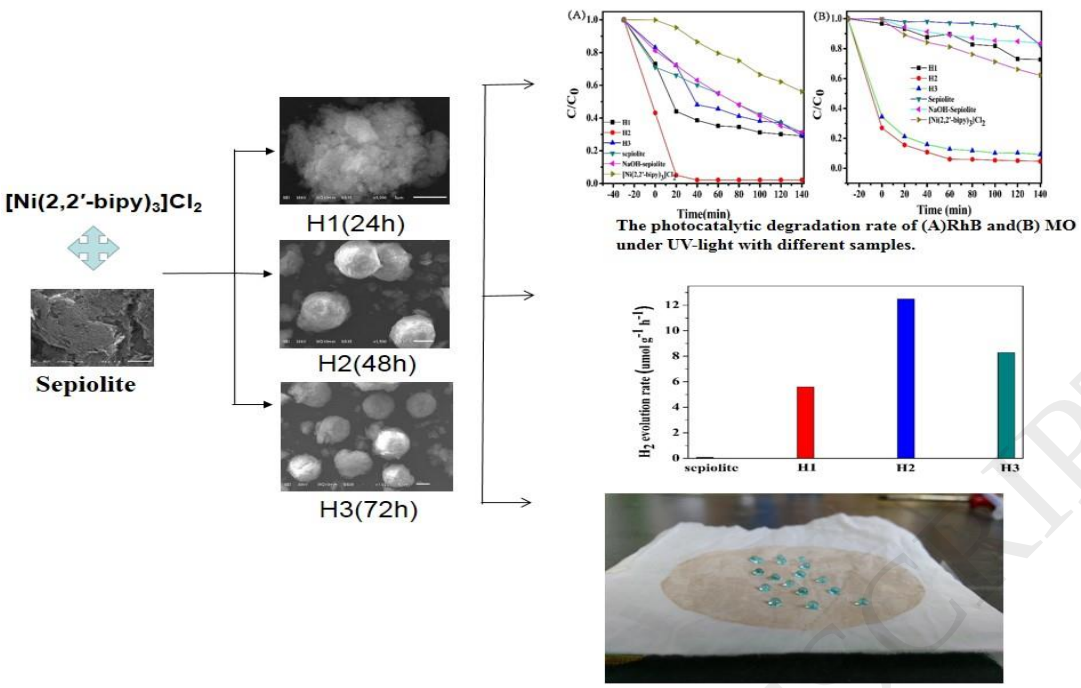

The photocatalytic degradation rate of (A)RhB and(B) MO under UV-light with different samples.

Research Highlights

- $Ni(2,2'\text{-bipy})_3]Cl_2$ /sepiolite was successfully prepared by hydrothermal method.
- $Ni(2,2'\text{-bipy})_3]Cl_2$ /sepiolite has the excellent photocatalytic for dye degradation and hydrogen evolution. .
- $Ni(2,2'\text{-bipy})_3]Cl_2$ /sepiolite possess extraordinary superhydrophobic and superoleophilic properties.
- $Ni(2,2'\text{-bipy})_3]Cl_2$ /sepiolite has the excellent oil–water separation abilities.

ACCEPTED MANUSCRIPT

Abstract

Novel $[Ni(2,2'\text{-bipy})_3]Cl_2$ activated sepiolite cla y composites have been successfully synthesized by a hydrothermal reaction method. The activated clays are endowed with much higher photocatalytic abilities than the raw one. Degradation ratios of rhodamine B and methyl orange under UV light were found up to 99.8% and 95.4% within 120 min. Beside efficient dye degradations, a high H_2 evolution rate of 12.5 umol/g/h was reached by using the $[Ni(2,2'\text{-bipy})_3]Cl_2$/sepiolite composite as the catalyst. Coating the as-synthesized material on surfaces leads to extraordinary superhydrophobic and superoleophilic properties. The cheap materials can be widely used in photocatalytic water purification and/or oil-water mixture separations.

Keywords: Sepiolite; $[Ni(2,2'\text{-bipy})_3]Cl_2$; Photocatalytic; Oil–water separation

1. Introduction

Belonging to the porous inorganic-organic hybrid material category, the newly-developed coordination compounds have attracted tremendous attentions due to their diverse and easily tailored structures[1-5], and potential applications in various fields such as catalysis[6-9] , separation[10-12], gas storage[13-16], carbon dioxide capture[17,18], etc[19,20]. Recent researches

ACCEPTED MANUSCRIPT

further showed that some coordination compound materials also possessed superior photocatalytic abilities for water purifications and hydrogen evolution. Therein, organic pollutants were degraded under UV/visible/UV-Visible irradiations, and hydrogen, the most promising clean fuel, was also produced. [21-24]

Despites successes of synthesizing functional metal-organic frameworks in these works, the low-cost nickel (II) polypyridyls reagents have not been considered as good photosensitizers. This is due to activation difficulties and lack of proper carriers. The former blockage arises from very short lifetimes of the metal-to-ligand charge transfer (MLCT) states, which are typically within a range of picoseconds to nanoseconds. However, a feasible substitution of bipyridine ligands to CN-ligands was reported in an early work of Ferrere[25], because of driving force changes of the electron injection from the lower energy MLCT band. This mechanism may work when using the nickel (II) polypyridyls in photochemical application and hydrogen evolution. The latter drawback requires recovery of coordination compounds powder in industrial implementation. Thus, proper carriers and synthetic routes are needed.

Indeed, in synthetic photocatalyst designs, numerous works are devoted to developing combinations with different functional composites

ACCEPTED MANUSCRIPT

to reach high catalytic activities and chemical stabilities. The synthesized composites can be semiconductor heterojunctions[26], supported layers[27], and morphologically modified species[28]. The coordination compound's integrations to/or annexes on supporting materials can enlarge application scopes due to the hosts' peculiar properties and structures as well as their abundance and low-cost merits[29,30]. In this regard, sepiolite is a promising supporting material thanks to its abundance, nontoxicity and non-harmful features. The clay is composed of fibrous morphology and intra-crystalline channels. The chemical formula reads $Si_{12}Mg_8O_{30}(OH)(OH_2)_4 \cdot 8H_2O$ for the idea half-unit sepiolite cell and the large specific surface reaches more than 200 m^2/g[31-34]. Its individual block consists of two tetrahedral silica sheets and a central octahedral sheet containing magnesium, resulting in zeolite-like channels[35]. The unique pore structure with interior channels make the clay a good adsorbent and catalytic material following synergic effects of the nanoparticle support systems[36]. Besides dispersing attached accessories, sepiolite can also enhance reactivities of the combined catalysts. Aranda et al. found that sepiolite has a positive synergistic effect on the TiO_2 photocatalysis[37,38]. Further, sepiolite can immobilize Ag_3PO_4, and form the Ag_3PO_4-sepiolite composite. Robust photocatalytic activities were introduced in degradations of the 2,4-DCP model pollutant under visible

ACCEPTED MANUSCRIPT

light radiations[39]. Therefore, sepiolite is considered as a cheap but functional candidate among supporting materials for coordination compounds.

In this work, the $[Ni(2,2'\text{-bipy})_3]Cl_2$ activated sepiolite composites have been developed and then used in the decolouration of organic pollutant (such as Rhodamine B RhB, Methyl Orange MO) solutions under UV-light irradiation and photocatalytic water splitting reaction. To the best of our knowledge, it is the first report on $[Ni(2,2'\text{-bipy})_3]Cl_2$/sepiolite composites, despite of distinguishing properties of the nickel compounds and the clay supporting. Results showed that as-prepared sample degraded RhB/MO under UV-light irradiation with excellent efficiency. Moreover, the composites can be served as catalysts for hydrogen envolution from water under simulated sunlight. Coating organic frameworks with the active clay brought simultaneously superhydrophobic and superoleophilic properties for effective separation of the oil-water mixture. Besides a synthetic route for the multifunctional clay, this work explored physical mechanisms leading to the unique photocatalytic activity.

2. Experimental

2.1 Materials and synthesis

ACCEPTED MANUSCRIPT

The sepiolite clay in this study was obtained from Hunan Province, China. Other chemicals were of analytical grade and taken without further purification or modification.

Firstly, a certain amount of sepiolite was immersed into NaOH (1mol/L) and stirred for 30 min. The above solution was transferred into 100 mL Teflon-lined stainless steel autoclave and heated at 180℃for 24 h. The solid was filtered, dried at 70℃ for 8 h, and the resulted sepiolite was employed as the carrier in later synthesis.

The $[Ni(2,2'\text{-bipy})_3]Cl_2$ was prepared and purified following the reported steps[40]. A solution of 2,2'-bipyridine (0.984g, 6.3 mmol) was added in ethanol ($30cm^3$) with $NiCI_2{\cdot}6H_2O$ solution (0.499g, 2.1mmol) additive. The mixture was heated up slowly and stirred for 0.5 h. The product was filtered off and the filtrate concentrated by rotary evaporation to yield more solid. The combined solids were washed in ethanol and then dried in vacuum.

In a typical synthesis of $[Ni(2,2'\text{-bipy})_3]Cl_2$-activated sepiolite composites, 1.0 g of sepiolite powder was put into double distilled water, stirred for 10 min and then added with 0.600 g of $[Ni(2,2'\text{-bipy})_3]Cl_2$. After 30 min stirring, the above solution was transferred into 100 mL Teflon-lined stainless steel autoclave and heated at 180℃ for different durations of 24 h (H1), 48 h (H2) and 72 h (H3). After cooled to room

ACCEPTED MANUSCRIPT

temperature, the as-obtained solid substance was collected by centrifugation, washed for several times with absolute ethanol and deionized water, and dried at 80℃for 8 h.

Superhydrophobic surfaces were prepared via the well-established screen-printing method[43]. In the coating procedure, the sepiolite composites were suspended (1:2 wt%) in polydimethylsiloxane(PDMS) and blended afterwards. The $[Ni(2,2'\text{-bipy})_3]Cl_2$/sepiolite was printed through a sieved screen[41] on filter paper, commercially available glass (5 cm^2-10 cm^2) and filter cloths.

2.2 Characterization

The microstructures of the samples were investigated by X-ray diffraction (XRD) patterns collected from Rigaku Dmax/Ultima IV diffractometer. FTIR spectra were measured at a range of 400-4000 cm^{-1} at a step of 2 cm^{-1} and a KBr pellet. A Lambda 25 UV–vis spectrophotometer (Perkin-Elmer, USA) was employed to monitor absorption spectra of $[Ni(2,2'\text{-bipy})_3]Cl_2$/sepiolite during dye degradations under the UV light irradiation at a spectral range of 200–800 nm. Morphologies analysed by the Scanning Electron Microscopy (SEM) (JEOL JSM-6700F). X-ray photoelectron spectroscopy (XPS) was performed on a PHI 5300 with a monochromatic Mg Kα source to explore the element chemical states. Transmission electron microscopy

ACCEPTED MANUSCRIPT

(TEM) and high-resolution electron microscopy (HRTEM) images were taken using a JEOL JEM-2010 electron microscope. Nitrogen adsorption-desorption isotherms were obtained on a nitrogen adsorption apparatus (TRISTAR II 3020, USA). UV-vis diffuse reflectance spectra were obtained for the dry pressed disk samples with a UV-visible spectrophotometer (UV-2550, Shimadzu, Japan) using $BaSO_4$ as the reference. The spectra were recorded at room temperature in the range of 200-800 nm. Photoluminescence (PL) spectroscopy was performed on a LS55 fluorescence spectrometer at an excitation wavelength of 375 nm. Intermediates of RhB degradation were identified using MS (autoflex, Germany).

2.3 Evaluation of photocatalytic activity

The photochemical reactor has an optical quartz glass beaker surrounded by a water jacket to keep the reaction at room temperature. The photocatalytic activities of the $[Ni(2,2'\text{-bipy})_3]Cl_2$/sepiolite catalysts were evaluated by the degradations of RhB and MO. Typically, 100 mg of the as-prepared photocatalyst composite was stirred in 100 mL aqueous dye solution (10 mg/L). Before the experiment, the suspension was stirred in the dark for 30 min to reach adsorption equilibrium. During the irradiation, 3 mL of the suspension was extracted at a certain time interval. The solution was centrifuged, and the concentration of RhB and

ACCEPTED MANUSCRIPT

MO were analysed by the UV–vis spectrophotometer. The RhB and MO concentrations were evaluated initially and at fixed time intervals to study degradation kinetics. The efficiency was calculated using the following equation [42]

$$\eta = \frac{C_0 - C_i}{C_0} \cdot 100 \quad (1)$$

where C_0 is the initial concentration and C_i the concentration after a fixed time.

Photocatalytic hydrogen evolution on the as-prepared catalysts was evaluated on a side-irradiated gas-closed system. In each experiment, 50 mg of sample was dispersed into 50 mL of aqueous solution, which comprised of 10 vol % triethanolamine (TEOA) as the sacrificial reagent. Before the light irradiation, the sealed reaction system was purged with the high-purity N_2 gas for 0.5 h to remove the dissolved air in the aqueous solution. 3.0 wt% Pt was loaded onto the as-prepared photocatalysts as a co-catalyst from H_2PtCl_6 aqueous solution via *in situ* photodeposition. A 300 W Xe arc lamp was used as light source. The amount of H_2 evolution was measured by using gas chromatograph (GC-6890A).

2.4 Wettability measurement

ACCEPTED MANUSCRIPT

The contact angle (CA) was measured on an optical contact anglemeter (250-F1) at room temperature. Superhydrophobic surface was prepared by screen-printing method. The film was dried naturally. Water droplets were carefully dripped onto the surfaces, and the average value of five measurements obtained at different positions in the samples was used as the final CA.

3. Results and discussion

3.1 Material characterizations

In total, three samples of $[Ni(2,2'\text{-bipy})_3]Cl_2$/sepiolite have been synthesized and named as H1 (24h), H2 (48h) and H3 (72h), respectively. Fig. 1 shows the XRD patterns of the samples. It can be seen that main diffraction peaks are very sharp in all samples, denoting well crystallizations of the samples. H1, H2 and H3 have the same pattern features as the NaOH treated sepiolite and a very low content of $[Ni(2,2'\text{-bipy})_3]Cl_2$ (Fig. 1A-D). Compared with the raw clay, a small shift of the main peak was observed in base treated one. This may be attributed to a minor change in the crystal structure subjected to the leaching of Si^{4+} during the reactions between sepiolite and NaOH.

Chemical compositions in the final products are identified via Fourier transform infrared spectroscopy (FT-IR). The spectra of [Ni(2,2′-

ACCEPTED MANUSCRIPT

bipy)$_3$]Cl$_2$/sepiolite catalysts with different hydrothermal reaction time were shown in Fig. 2 along with these from the natural and base treated sepiolite. The band at 3687 cm^{-1} corresponds to stretching vibrations of the hydroxyl groups (νOH). The -OH attaches to the octahedral Mg ions located at the interior blocks of the natural sepiolite and [Ni(2,2′-bipy)$_3$]Cl$_2$/sepiolite. The band at 3622 cm^{-1} is assigned to H-O-H stretching vibrations of water molecules weakly bonded to the Si-O surface in both samples. The broad band at 3411 cm^{-1} observed in each samples comes from the H-O-H vibrations of the adsorbed water. Bands at the 1200−400 cm^{-1} range are characteristic peaks of silicate while bands centred at 1028 and 465 cm^{-1} are due to Si-O-Si vibration. Bands at 1216, 1083 and 978 cm^{-1} are ascribed to Si-O bonds, and bands at 690 and 642 cm^{-1} to Mg-OH bond vibrations[43]. In the FTIR spectrum of pure [Ni(2,2′-bipy)$_3$]Cl$_2$, strong peaks at 1578.8 cm^{-1} changes to a weak absorption peak at 1606~1385cm^{-1}. Peaks at 769 cm^{-1} are due to C-H bending vibration of the benzene ring.

To elucidate surface compositions and chemical states, samples of [Ni(2,2′-bipy)$_3$]Cl$_2$/sepiolite catalysts with hydrothermal reaction time for 48h was chosen as a model for XPS analysis, and the results are shown in Fig. 3. The [Ni(2,2′-bipy)$_3$]Cl$_2$/sepiolite composite catalysts possess N, C, O, Mg, Si ,Cl and Ni elements (Fig. 3A). Signals from C, N, and Ni are

ACCEPTED MANUSCRIPT

well attributed to $[Ni(2,2'\text{-bipy})_3]Cl_2$, and these of Mg and Si are from sepiolite. As shown in Fig. 3B and C, the C 1s peak locates at 283.6 eV, and N 1s at 399.05 eV. In Fig. 3D, peaks of at 855.4 and 873.3 eV are attributed to $2p_{3/2}$ and $2p_{1/2}$ of the Ni^{2+} ions. The XPS analysis is consistent with FT-IR results, and further confirms the coexistence of $[Ni(2,2'\text{-bipy})_3]Cl_2$ in the $[Ni(2,2'\text{-bipy})_3]Cl_2$/sepiolite composite catalysts.

Fig. 4 depicts SEM images of the raw and activated sepiolite. The natural sepiolite is an aggregation of flakes with fibre and lamellar structure. Fibers stick together because of no pretreatment of dispersing was performed for the raw clay (Fig. 4A). The sepiolite composites activated by $[Ni(2,2'\text{-bipy})_3]Cl_2$ are shown in Fig. 4B, C and D. Obvious differences in morphology and microstructure are found between the natural and activated sepiolite. Different from irregular fiber forms in the raw clay, a microspherical morphology was achieved on the blocky-textured sample treated at 24h (Fig. 4B). It is worth mentioning that almost all sepiolite composites aggregated in form of small spherical particles and no other morphologies were observed. After 48h and 72h hydrothermal reactions, the composites are microspheres with an average diameter of 20 um (Fig. 4C and D). These results suggest that the hydrothermal reaction time have a significant impact on the morphologies and microstructure of the final products. Further insight into the

ACCEPTED MANUSCRIPT

morphology and microstructure of the as-synthesized [Ni(2,2′-bipy)$_3$]Cl$_2$/sepiolite catalysts was obtained through TEM determinations as depicted in Fig. 4E and HRTEM in Fig. 4F. The resulted microspheres are aggregations of large-scale sepiolite nanoplates among which the [Ni(2,2′-bipy)$_3$]Cl$_2$ nanoparticles were formed. The nanoplates have the widths between 200–800 nm and [Ni(2,2′-bipy)$_3$]Cl$_2$ nanoparticles between 10–60 nm. The TEM determination is consistent with the SEM observation. The HRTEM image of [Ni(2,2′-bipy)$_3$]Cl$_2$ nanoparticles in Fig. 4F presents the lattice fringes with a d-spacing of 0.369 nm.

We further studied the bandgap, porosity and luminescent properties of the samples. The bandgap energies of the [Ni(2,2′-bipy)$_3$]Cl$_2$/sepiolite composites were evaluated via UV-vis diffuse reflectance spectra as depicted in Fig. S1A. By extrapolating $(\alpha hv)^2$ to 0 (Fig. S1B) and converting wavelength to energy, a value of 3.65 eV (340 nm) was obtained for the activated clays as the main bandgap. This result suggests the UV light be able to trigger photonexcitations of the electrons within the samples. The specific surface areas (SSAs) and porosities of samples were tabulated in Table S1. The SSA increases with the [Ni(2,2′-bipy)$_3$]Cl$_2$ content due to presence of the pNi(2,2′-bipy)$_3$]Cl$_2$ nanoparticles, while the nanopore sizes keep unchanged among these samples. The photoluminescence (PL) spectra of the samples by the 375

ACCEPTED MANUSCRIPT

nm incident light in Fig S2. Generally speaking, the incident light cannot induce main photoexcitation in sepiolite due to the lower energy than the bandgap. However, the heterojunctional composites own several bandgaps after combining the $[Ni(2,2'\text{-bipy})_3]Cl_2$. Consequentially, PL spectra were produced after photoexcitation of electrons therein. The intensity of PL spectra in NaOH-sepiolite is highest, indicating that the separation efficiency of the photoinduced charge carriers is lowest. When $Ni(2,2'\text{-bipy})_3]Cl_2$ adhered to the sepiolite, the intensity of PL spectra decreased. In $[Ni\ (2,2'\text{-bipy})_3]Cl_2$ /sepiolite composite, the intensity of PL spectra is arranged as H2 < H3 < H1, meaning that the H2 exhibited best photocatalytic activity.

3.2 Photocatalytic activities

Photocatalytic activities of the as-synthesized samples were evaluated by degradations of RhB and MO as model pollutants under UV-light irradiation. Results of degradation efficiencies were graphed in Fig. 5. Adsorption equilibriums were reached at 30 min as shown by Fig S3. The RhB diminished gradually (Fig. 5A) and the photodegradation efficiencies were 71.6%, 99.8% and 70.9% for H1， H2 and H3, respectively (Table S2). Similarly, the absorption peak of MO at 463 nm decreased with irradiation time (Fig. 5B). The photodegradation efficiencies of MO were 27.4%, 95.4% and 90.1% for H1, H2 and H3,

ACCEPTED MANUSCRIPT

respectively. To test photocatalyst reusability, we conducted recycling experiments for the H2 sample. As shown in Fig. 5C and D, the RhB photodegradation efficiency of the catalyst decreases from 99.8% to 60% after four runs of 140 min each, and MO photodegradation from 95.4% to 46%. However, the XRD pattern of the recycled H2 after four cycles of photodegradation testing remains consistent with that of the fresh one in Fig S5, further confirming excellent stability of the samples.

We also compare the present catalysts to state-of-the-art ones in dye removals. First, the as-synthesized samples possess much better photocatalytic activities than the raw sepiolite for degrading RhB and MO in all degradation tests (see details in the Supporting Information). Using H2 as the catalyst, the MO and RhB concentrations dropped to ~5% and ~15% after 20 minutes of UV irradiation. The degrading rates are higher than these from synthetic photocatalysts such as $BiVO_4$[44], Sb_2WO_4[45] and comparable to the heterojunction bismuth oxyhalides[46]. The effective catalytic ability from the cheap clay is most probably due to smaller particle size and higher surface area of the treated sample. Such a morphological feature increased the contact area with dyes in solutions.

To explore the photocatalytic performance of these complexes in stimulated sunlight, the photocatalytic H_2 evolution (PHE) over various samples was investigated under stimulated sunlight. As shown in Fig. 5E,

ACCEPTED MANUSCRIPT

all of the [Ni (2,2′-bipy)$_3$]Cl$_2$ /sepiolite composites exhibit higher H_2 evolution activity than the raw sepiolite. Especially, H2 has the maximum PHE rate of 12.5 μmol $g^{-1}h^{-1}$, which indicated [Ni (2,2′-bipy)$_3$]Cl$_2$ could enhance photocatalytic activity. As shown in Fig 5F, after 24 h hydrogen production, the average of the hydrogen production was kept to the same value of 12.5 μmol $g^{-1}h^{-1}$. The photocatalysis was very stable. The [Ni (2,2′-bipy)$_3$]Cl$_2$ /sepiolite complex tuned the broadband gap of sepiolite and immobilized the soluble of [Ni (2,2′-bipy)$_3$]Cl$_2$. The PHE result is in line with the degradation of dyes. Indeed, dye removal and PHE undergo similar processes of water oxidization at the beginning. Difference remains at the further reaction path of the hydrogen radicals. In the dye removal, these radicals are recombined with oxygen or hydroxyl radicals, while in the PHE forming H_2 gas due to lack of oxidative radicals taken by the sacrifices.

To analyze the intermediates and final products of the RhB removal, the RhB solutions undergone photocatalytic reaction for 0, 1 and 2 h were investigated by mass spectrometry (MS). As shows in Fig S6 and Fig S7, the products collected from the solution with light irradiate for 1 h owns the m/z ratio of 415, 387, 359, and 331, which might be attributed to the de-ethylation process during the degradation of RhB. Moreover, when the

ACCEPTED MANUSCRIPT

light irradiate for 2 h the small m/z ratio including 172, 152, 122 and 102 could be assigned to opening-ring reaction from large molecules. Thus, the degradation of RhB in the presence of $[Ni(2,2'\text{-bipy})_3]Cl_2$/sepiolite includes three processes of deethylation, opening-ring, and mineralization.

We further studied photocatalytic mechanism of the coordination compounds activated sepiolite. Adsorption and photocatalytic degradation are the two major processes as shown in Fig. 6. Moreover, the experiments of radicals capture were carried out by adding 1 mmol potassium iodide (KI, a quencher of h^+), 1 mmol isopropanol (IPA, a quencher of •OH), and 1 mmol benzoquinone (BQ, a quencher of $\bullet O_2^-$), respectively[47-50]. At the presence of the potassium iodide (1mmol), the degradation of RhB was suppressed, indicating the participation of the h^+ in the photocatalytic reaction. When benzoquinone (1mmol) was added, the degradation of RhB changed substaintially, indicating that $\bullet O^{2-}$ was important in the photocatalytic process. However, when isopropanol was added, the change of RhB concentration was negligible. The above results demonstrate that $\bullet O^{2-}$ and h^+ were the main active species for the degradation of the organic pollutants with $[Ni(2,2'\text{-bipy})_3]Cl_2$/sepiolite catalysts under UV irradiation.

We also estimated the band alignment of the activated complex by

ACCEPTED MANUSCRIPT

studying the valance band of the sepiolite and $[Ni(2,2'\text{-bipy})_3]Cl_2$. Fig. S8 depicts the ultraviolent photoelectron spectra from which the binding energy of sepiolite and $[Ni(2,2'\text{-bipy})_3]Cl_2$ were calculated to 3.2 eV and 2 eV, respectively. Combined with UV–vis diffuse reflectance (Fig.S1) and PL results, the band alignment of the activated complex was shown in Fig S8, with respect to system's Fermi level. Apparently, both the VBM (valence band maximum) and CBM (conduction band maximum) of the clay are lower than these from the $[Ni(2,2'\text{-bipy})_3]Cl_2$, leading to possible charge transfers between these two counterparts. The lower binding energy of $[Ni(2,2'\text{-bipy})_3]Cl_2$ further explicates the photoexcitation by the 375 nm source for the PL production.

Following the electronic structure determination, the photocatalytic mechanism of $[Ni(2,2'\text{-bipy})_3]Cl_2$ /sepiolite composite was proposed and showed in Fig. 7. Since sepiolite has lower CB positions than $[Ni(2,2'\text{-bipy})_3]Cl_2$, the photogenerated electrons (e^-) in the CB of $[Ni(2,2'\text{-bipy})_3]Cl_2$ transfer to the CB of sepiolite. Meanwhile, the photogenerated electrons in the CB of sepiolite reduces the adsorbed O_2 to yield $\bullet O_2^-$, which was a powerful oxidative specie for RhB and MO degradation. However, the VB levels of $[Ni(2,2'\text{-bipy})_3]Cl_2$ were not positive enough so that it doesn't have sufficient oxidation ability to drive the oxidation process, while sepiolite has higher VB levels which can transfer H_2O to

ACCEPTED MANUSCRIPT

•OH. The comparison of •OH/H_2O potential (ca. 2.27 V) suggests that photogenerated holes (h^+) in the CB of sepiolite transfer to the CB of [Ni(2,2′-bipy)$_3$]Cl_2.

3.3 Wettability

Micro-spherical particles of the activated clay, once deposited on proper substrates, may have special wettability due to the morphological uniqueness. Thus, films of the as-synthesized [Ni(2,2′-bipy)$_3$]Cl_2/sepiolite catalysts were deposited on filter papers using a well-established screen-printing technique with the polydimethylsiloxane(PDMS) as adhesive[51]. Contact angles of 10 μL water droplets were depicted in Fig. 8. Measurements were performed without modification by low-surface-energy materials. The CA values of more than 150° were obtained when the pH values of the water droplets varied from 1.0 to 13.0. The as-prepared films have superhydrophobicity at a wide pH range (within experimental error, at all pH values). The superhydrophobicity applies for pure water, and corrosive liquids including acidic, basic and some aqueous salt solutions. It is well known that the raw filter paper is hydrophilic. Therefore, wettability of the filter paper modified by [Ni(2,2′-bipy)$_3$]Cl_2/sepiolite samples is improved substantially and becomes superhydrophobicity without using oriented materials or stearic acid.

ACCEPTED MANUSCRIPT

Similar to previous studies[52-55] of analogous materials, material morphology was attributed to the dominant factor for a superhydrophobic surface. Additionally, the creation of micro/nanorods, which favours slower growing planes and therefore a lower surface energy, also contributes. We also extended usability of the activated clay, and coated a flat glass substrate with the as-prepared samples. A large CA value of more than 150° was obtained (Fig. S9, Supporting Information). The $[Ni(2,2'\text{-bipy})_3]Cl_2$/sepiolite catalysts were also deposited on filter cloth using the well-established screen-printing technique with the PDMS adhesive. Because the unevenness on the surface of the filter cloth, we cannot accurately determine water contact angle. Instead, we dropped water on the surface in the static tests (Fig. S10, Supporting Information) and later in oil-water separation test (video S5 and S7, Supporting Information). From above evidences, this method could be applied to other substrates, such as filter cloth, copper mesh and stainless steel mesh, to fabricate superhydrophobic surfaces.

To evaluate stability against pressure-induced wetting, a series of tests were conducted. The mechanical stability of film was evalutated by cellophane tape method. The super-hydrophobic filter paper films surface remained superhydrophobic after multiple paste and detachment processes as shown in Fig. 9A. In general, the anti-wetting property and

ACCEPTED MANUSCRIPT

the number of abrasions do not fit to each other. However, in the present work, filter paper films could still keep highly hydrophobic after 20 cycles of abrasion. And the CAs for water droplets (PH=7) placed on the filter paper film surface decreased slight from 160° in the initial state to 140°. To investigate robustness of the super-hydrophobic filter paper film, methylene blue (MB) was dissolved into deionized water and used as a model dust, then a droplet of solution was dripped onto the surface at an inclination angle of 20°. Fig. 9B-D show snapshots where MB-dyed water droplet slide off the coated film damaged by scissor scratches. It is obvious that water rolled off easily from the superhydrophobic coating without any viscous damping. This was due to the low surface energy of $[Ni(2,2'\text{-bipy})_3]Cl_2$/sepiolite catalysts. Combining with rough structures of the samples, we can confirm liquid and solid - liquid interface that a high ratio of trapped air appeared, similar to the case of biomimicked surfaces[56]. Even after mechanical damages[57], the painted surfaces on all kinds of substrates still maintained a good network-load performance. Furthermore, the PDMS' good adhesion minimizes the sample loss[58]. As shown in Fig. 9E-L, the painted surfaces were still clean and dry even after knife scratch and then water drop (Video S1-S2 in the Supporting Information).

Both natural and synthetic superhydrophobic surfaces are believed to

ACCEPTED MANUSCRIPT

achieve self-cleaning due to "lotus effect"[59,60]. The lotus effect typically refers to the removal of the contaminating particles by impacting and/or rolling water droplets[61]. The superhydrophobicity is important because of the associated large contact angle and small hysteresis, which promotes the rolling motion carrying away contaminants[62]. The self-cleaning tests of the as-prepared superhydrophobic coating surface (Fig. 10 and Video S3) was implemented with MO powder as a simulating pollutant[63]. Video S3 shows the fast process of removal of the MO powder by water droplets and the surface recovery of its superhydrophobicity. The MO simulated pollutant powders were scattered all over the surface and then use disposable test tubes that drip water on the contaminated fabric. During the sliding process, dusts were immediately pasted on the surface of the water droplets, dissolved and carried away by the gravitational force. This observation confirmed that the high water surface tension and low surface energy of $[Ni(2,2'\text{-bipy})_3]Cl_2$/sepiolite played an important role in self-cleaning. In this test, we also use the non-dissolvable MnO_2 powder as a model dust/contaminant to test the self-cleaning function of the as-prepared superhydrophobic coating surface(Fig. S11, Supporting Information). The dusts were removed by the water droplets.

The oil wettability of the as-prepared film was examined through the contact angle measurements. Fig. 11A–C show a drop of octane became

ACCEPTED MANUSCRIPT

nonvisible immediately on the as-prepared film. The octane spread quickly on the coating and absorbed thoroughly within about 1.0 s without leaving any residue (see details in the Supporting Information video S4 and S5). The intrusion pressure was calculated to 0.04kPa by using the equation of $P_E = \rho gh$. The flux keeps a relative high level of 596 L m^{-2} h^{-1}.[64-66] This indicates that the as-prepared film has an excellent superoleophilic property. Combining with superhydrophobicity, such coatings have potential applications in life science and materials processing, e.g., oil-water mixture separation, self-cleaning materials and drag reducing materials, etc [67-69].

The oil-water separation efficiency was studied as shown in Fig. 11E-F. When the mixture of water (dyed with methyl blue) and dichloromethane (dyed with Sudan Ⅲ) was poured onto the device, the latter sank to the bottom of the device due to its larger density than water. Driven by gravity, Sudan Ⅲ-dyed dichloromethane was popped up in the device, penetrated through the filter paper/filter cloth and owed down to the beaker below. Meanwhile water retained on the surface of the filter paper. Clear distinction of different liquids proves the excellent ability for oil–water separation of the $Ni(2,2'\text{-bipy})_3]Cl_2$/sepiolite coated film. Furthermore, the whole separation process was completed within a few min (see details in the Supporting Information video S6 and S7). The

ACCEPTED MANUSCRIPT

separation ability is available for other organic-water mixtures. A variety of oil/water mixtures (50% v/v) also have been successfully separated through the same process including octane, hexane, and rapeseed oil. The separation efficiency of a variety of oils was expressed by the water permeation coefficient (η/%). It was calculated by $\eta(\%)=(m_1/m_0)\times100\%$, where m_1 separation represents the weight of water after each separation, and m_0 denotes the weight of water in the initial oil-water mixtures[70,71]. The separation efficiency of the coated filter paper/filter cloth was calculated to 99% for the octane−water mixture and above 99% for other oils. Moreover, the obtained functional film can retain its high oil–water separation efficiency even after five cycles of oil–water separations. These results indicated that the as-prepared superhydrophobic film is a promising candidate for oil-spill clean-up.

Water and oil wettability of the activated clay are also compared with these of state-of-the-art materials. Here the water CAs, in general, are larger than values on hydrophobic but vulnerable polymer replica[72], and on the titania coated meshes. The hydrophobic and superoleophilic properties of films coated with the $Ni(2,2'\text{-bipy})_3]Cl_2$/sepiolite (especially H2) are also superior to films coated with latest-developed synthetic crystals such as porous $Cu_3(BTC)_2\cdot3H_2O$ [73], $BaMnF_4$ [74], ZnC_4O_4 [75], etc. Besides large water CA at pH=7, the H2 hydrophobicity is resistant

ACCEPTED MANUSCRIPT

against corrosions as shown in Fig. S9. In addition, the abundance of the carrying frame and low-cost nature further distinguish the present samples from the aforementioned peers.

4. Conclusions

In summary, the naturally occurring sepiolite clay has been successfully activated as a bifunctional catalysts after $[Ni(2,2'\text{-bipy})_3]Cl_2$ treatments. The hydrothermal reaction time of the precursors has a significant effect on the morphology, photocatalytic activity and superhydrophobic property of the products. The as-prepared $[Ni(2,2'\text{-bipy})_3]Cl_2$-activated sepiolite composite not only exhibited excellent photocatalytic degradation and hydrogen envolution, but also showed a significant superhydrophobic property (CA>150°). The photocatalytic abilities of the activated sepiolite clay are much higher than the raw counterpart, and comparable with the synthetic but dedicated compounds. The superhydrophobic surface retained its wettability and self-cleaning property even under scratch and survived from multiple attachment-detachment processes of the scotch tape. Because of the superhydrophobic/superoleophilic properties, the printed surface benefits oil−water separation processes with excellent separation efficiency. Further, the oil−water separation coating still kept high separation efficiency after 5 cycles.

ACCEPTED MANUSCRIPT

Besides its low-cost and efficient photocatalytic perspectives in water purification, the $[Ni(2,2'\text{-bipy})_3]Cl_2$-activated sepiolite is also promising in manufacturing superhydrophobic surfaces that will work in harsh and oily environments, such as external wall coating and oil−water separation material.

Acknowledgements

The authors acknowledge with thanks the financial support of the National Natural Science Foundation of China (21601149), Scientific Research Fund of Hunan Provincial Education Department, China (16B253), and Hunan 2011 Collaborative Innovation Center of Chemical Engineering & Technology with Environmental Benignity and Effective Resource Utilization. W. Cao thanks financial supports from Academy of Finland (311934) and the Oulu University Strategic Grant. Authors thank A. A. Ovichinnikova for language improvement.

ACCEPTED MANUSCRIPT

ACCEPTED MANUSCRIPT

References

1 J.M. Hao, Y.N. Zhao, H.H. Li, C.L. Ming, G.H. Cui, Synthesis, Structures, and Characterization of Two d10 Metal Coordination Polymers With a Flexible Bis(triazole) Ligand, Inorg. Met. Org. Nanomet. Chem. 45 (2015) 947-951.

2 C.L. Ming, Z.C. Hao, B.Y. Yu, K. Van Hecke, G. H. Cui, Synthesis, Structures, and Catalytic Properties of Three New Metal–Organic Coordination Polymers Constructed from Flexible Benzimidazole-Based and cis-1,2-Cyclohexanedicarboxylate Synthons, J Inorg Organomet Polym Mater. 25 (2015) 559-568.

3 L. Qin，G.Y Li，J Zheng，S.L. Xiao，G.H. Cui, Two 3D Supramolecular Architectures from Ag(I) Coordination Polymers Constructed by Flexible Bis(benzimidazolyl)butane Ligand, J Inorg Organomet Polym Mater. 23 (2013) 1266-1273.

4 S.L. Xiao, L. Qin, C.H. He, X. Du, G.H. Cui, Synthesis, Characterizations and Luminescent Properties of Two Cadmium(II) Coordination Polymers Derived from Bis(Benzimidazole)-Based Ligands, J. Inorg. Organomet. Polym Mater. 23 (2013) 771-778.

5 J.M. Hao, Y.N. Zhao, B.Y. Yu, K. Van Hecke, G. H. Cui, Structural diversity of transition-metal coordination polymers derived from

ACCEPTED MANUSCRIPT

isophthalic acid and bent bis(imidazole) ligands, Trans. Met. Chem. 39 (2014) 741-753.

6 J. Lee, O.K. Farha, J. Roberts, K.A. Scheidt, S.T . Nguyen, J. T.Hupp, Metal-organic framework materials as catalysts, Chem Soc Rev. Chem.Soc. Rev. 38 (2009) 1450-1459.

7 Y. Ma, X. Wu, G. Zhang, Core-shell Ag@Pt nanoparticles supported on sepiolite nanofibers for the catalytic reduction of nitrophenols in water: Enhanced catalytic performance and DFT study, Appl. Catal. B: Environ. 205(2016)262-270.

8 M. Ying, G. Zhang, Sepiolite nanofiber-supported platinum nanoparticle catalysts toward the catalytic oxidation of formaldehyde at ambient temperature: Efficient and stable performance and mechanism, Chem. Eng. J. 288 (2016) 70-78.

9 Y. Gao, H. Gan, G. Zhang, et al, Visible light assisted Fenton-like degradation of rhodamine B and 4-nitrophenol solutions with a stable poly-hydroxyl-iron/sepiolite catalyst, Chem. Eng. J. 217 (2013) 221-230.

10 J.R. Li, R.J. Kuppler, H.C. Zhou, Selective gas adsorption and separation in metal–organic frameworks, Chem. Soc. Rev. 38 (2009) 1477-1504.

ACCEPTED MANUSCRIPT

11 J.R. Li, J. Sculley, H.C. Zhou, Metal–organic frameworks for separations, Chem. Rev. 112 (2011) 869-932.

12 J.R. Li, Y. Ma, M.C. McCarthy, J. Sculley, J. Yu, H.K. Jeong, P.B. Balbuena, H.C. Zhou, Carbon dioxide capture-related gas adsorption and separation in metal-organic frameworks, Chem. Rev. 255 (2011) 1791-1823.

13 S. Ma, H.C. Zhou, Gas storage in porous metal-organic frameworks for clean energy applications, Chem. Commun. 46 (2010) 44-53.

14 L.J. Murray, M. Dinca, J.R. Long, Hydrogen storage in metal–organic frameworks, Chem. Soc. Rev. 38 (2009) 1294-1314.

15 N.L. Rosi, J. Eckert, M. Eddaoudi, D.T. Vodak, J. Kim, M.O. Keeffe, O.M. Yaghi, Hydrogen storage in microporous metal-organic frameworks, Science. 300 (2003) 1127-1129.

16 M. Peplow, Materials science: The hole story, Nature. 520 (2015) 148-150.

17 K. Sumida, D.L. Rogow, J. A. Mason, T.M. McDonald, E.D.Bloch, Z.R. Herm, T.H. Bae, J.R. Long, Carbon dioxide capture in metal–organic frameworks, Chem. Rev. 112 (2011) 724-781.

18 M.C. So, G.P. Wiederrecht, J.E. Mondloch, J.T. Hupp, O.K. Farha, Metal–organic framework materials for light-harvesting and energy transfer, Chem. Commun. 51 (2015) 3501-3510.

ACCEPTED MANUSCRIPT

19 W. Cai, C.C. Chu, G. Liu, Y. X. J. Wang, Metal–Organic Framework-Based Nanomedicine Platforms for Drug Delivery and Molecular Imaging, Small. 11 (2015) 4806-4822.

20 J.M. Hao, B.Y. Yu, K. Van Hecke, G.H.Cui, A series of d10 metal coordination polymers based on a flexible bis(2-methylbenzimidazole) ligand and different carboxylates: synthesis, structures, photoluminescence and catalytic properties, CrystEngComm. 17 (2015) 2279-2293.

21 C.C. Wang, J.R. Li, X.L .Lv, Y.Q. Zhang, G. Guo, Photocatalytic organic pollutants degradation in metal–organic frameworks, Energy Environ. Sci. 7 (2014) 2831-2867.

22 S. Wang, X. Wang, Multifunctional metal–organic frameworks for photocatalysis, Small. 11 (2015) 3097-3112.

23 T. Zhang, W. Lin, Metal-organic frameworks for artificial photosynthesis and photocatalysis, Chem. Soc. Rev. 43 (2014) 5982-5993.

24 H.P. Jing, C.C. Wang, Y.W. Zhang, P. Wang, R. Li, Photocatalytic degradation of methylene blue in ZIF-8, RSC Adv. 4 (2014) 54454-54462.

25 S. Ferrere, New Photosensitizers Based upon $[Fe(L)_2(CN)_2]$ and $[Fe(L)_3]$ (L = Substituted 2,2‘-Bipyridine): Yields for the

ACCEPTED MANUSCRIPT

Photosensitization of TiO_2 and Effects on the Band Selectivity, Chem. Mater. 12(2000)1083-1089.

26 H. Tada, Y. Konishi, A. Kokubu, S. Ito, Patterned TiO_2/SnO_2 bilayer type photocatalyst. 3. Preferential deposition of Pt particles on the SnO_2 underlayer and its effect on photocatalytic activity, Langmuir. 20 (2004) 3816-3819.

27 C.H. Wu, J.F. Shr, C.F. Wu, C.T. Hsieh, Synthesis and photocatalytic characterization of titania-supported bamboo charcoals by using sol–gel method, J. Mater. Process. Technol. 203 (2008) 326-332.

28 V.F. Stone, R.J. Davis, Synthesis, Characterization, and Photocatalytic Activity of Titania and Niobia Mesoporous Molecular Sieves, Chem. Mater. 10 (1998) 19959-65.

29 E.G. Garrido-Ramírez, B.K. G. Theng, M.L. Mora, Clays and oxide minerals as catalysts and nanocatalysts in Fenton-like reactions — A review, Appl. Clay Sci. 47 (2010) 182–192.

30 L.A. Galeano, M.Á. Vicente, A. Gil, Treatment of municipal leachate of landfill by Fenton-like heterogeneous catalytic wet peroxide oxidation using an Al/Fe-pillared montmorillonite as active catalyst, Chem. Eng. J. 178 (2011) 146–153.

31 M. Ugurlu, Micropor, Mesopor. Mater. 119 (2009) 276-283.

ACCEPTED MANUSCRIPT

32 F.M. Bautista, J.M. Campelo, D. Luna, J. Luque, J.M. Marinas, Vanadium oxides supported on TiO_2-Sepiolite and Sepiolite: Preparation, structural and acid characterization and catalytic behaviour in selective oxidation of toluene, Appl. Catal. A General. 325 (2007) 336-344.

33 J.Korosi, E. Bazso, V. Zollmer, A. Richardt, I. Dekany, Photocatalytic oxidation of organic pollutants on titania–clay composites, Chemosphere, 70 (2008) 538-542.

34 E. Sabah, M. Turan, M.S. Çelik, Adsorption mechanism of cationic surfactants onto acid- and heat-activated sepiolites, Water Res. 36 (2002) 3957-3964.

35 G. Li, L.J. Chen, B. Zhang, L. Yi, Novel Bi_2O_3 loaded sepiolite photocatalyst: Preparation and characterization, Mater. Lett. 168 (2016) 143-145.

36 L. Zou, Removal of VOCs by photocatalysis process using adsorption enhanced TiO_2–SiO_2 catalyst, Chem. Eng. Process. 45 (2006) 959–964.

37 S. Suarez, J.M. Coronado, R. Portela, J.C. Martin, M. Yates, P. Avila, B. Sanchez, On the preparation of TiO_2-sepiolite hybrid materials for the photocatalytic degradation of TCE: influence of

ACCEPTED MANUSCRIPT

TiO_2 distribution in the mineralization, Environ. Sci.Technol. 42 (2008) 5892-5896.

38 P. Aranda, R. Kun, M. A. Martín-Luengo, S. Letaïef, I. Dekany, E. Ruiz-Hitzky, Titania−Sepiolite Nanocomposites Prepared by a Surfactant Templating Colloidal Route, Chem. Mater. 20 (2008) 84-91.

39 T.H. Liu, X.J. Chen, Y.Z. Dai, L.L. Zhou, J. Guo, Synthesis of Ag_3PO_4 immobilized with sepiolite and its photocatalytic performance for 2,4-dichlorophenol degradation under visible light irradiation, J. Alloy. Compd. 649 (2015) 244-253.

40 A. Ozcan, E.M. Oncu, A.S. Ozcan, Adsorption of Acid Blue 193 from aqueous solutions onto DEDMA-sepiolite, J. Hazard. Mate. B129 (2006) 244-252.

41 Y. Chen, F. Li, W. Cao, T. Li, Preparation of Recyclable CdS Photocatalytic and Superhydrophobic Film with Photostability by Screen-printing Technique, J. Mater. Chem. A. 3 (2015) 16934-16940.

42 C. Yang, Y. Huang, T.H. Li, F. Li, ChemInform Abstract: Bi_2WO_6 Nanosheets Synthesized by a Hydrothermal Method: Photocatalytic Activity Driven by Visible Light and the Superhydrophobic Property with Water Adhesion, [J] Chem. 46 (2015) 2560-2564.

ACCEPTED MANUSCRIPT

43 J. MADEJOVA, FTIR techniques in clay mineral studies, Vib. Spectrosc. 31 (2003) 1-10.

44 S. Zhu, Q. Li, F. Li, W. Cao, T. Li, One-pot synthesis of Ag^{+} doped $BiVO_4$ microspheres with enhanced photocatalytic activity via a facile hydrothermal method, J. Mat. Sci. 92 (2016) 11-18.

45 C. Yang, X. Yang, F. Li, T. Li, W. Cao, Controlled synthesis of hierarchical flower-like Sb_2WO_6 microspheres: Photocatalytic and superhydrophobic property, J. Ind. Engi. Chem. 39 (2016) 93-100.

46 C. Yang, F. Li, T. Li, W Cao, Preparation and first-principles study for electronic structures of BiOI/BiOCl composites with highly improved photocatalytic and adsorption performances, J. Mol. Cat. A. 423 (2016)1-11.

47 L.S. Zhang, K.H. Wong, H.Y. Yip, C. Hu, J.C. Yu, C.Y. Chan and P.K. Wong, Effective photocatalytic disinfection of E. coli K-12 using AgBr-Ag-Bi_2WO_6 nanojunction system irradiated by visible light: the role of diffusing hydroxyl radicals, Environ. Sci. Technol. 44 (2010) 1392–1398.

48 R. Palominos, J. Freer, M.A Mondaca and H.D Mansilla. J. Photochem, Journal of Photochemistry and Photobiology A: Chemistry, Photobiol. A. 193 (2008) 139–145.

ACCEPTED MANUSCRIPT

49 Y. Li, J. Wang, H. Yao, L. Dang and Z. Li, Efficient decomposition of organic compounds and reaction mechanism with BiOI photocatalyst under visible light irradiation, J. Mol. Catal. A: Chem. 334 (2011) 116–122

50 T. An, J. An, H. Yang, G. Li, H. Feng and X. Nie, Photocatalytic degradation kinetics and mechanism of antivirus drug-lamivudine in TiO_2 dispersion, J. Hazard. Mater. 197 (2011) 229–236.

51 S.N. Yin, C.F. Wang, Z.Y. Yu, J. Wang, S.S. Liu, Tunable Janus colloidal photonic crystal supraballs with dual photonic band gaps, J. Mater. Chem. A. 2 (2014) 4178-4184.

52 A. Nakajima, A. Fujishima, K. Hashimoto, T. Watanabe, Preparation of transparent superhydrophobic boehmite and silica films by sublimation of aluminum acetylacetonate, Adv.Mater. 11 (1999) 1365-1368.

53 A. Nakajima, K. Hashimoto, T. Watanabe, Monatsh, Effect of repeated photo-illumination on the wettability conversion of titanium dioxide, J. Photochem. Photobio. A. 146 (2001) 129-132.

54 A.B.D. Cassie, Permeability to water and water vapour of textiles and other fibrous materials. Introductory paper, Discuss. Faraday Soc. 3 (1948) 239-243.

ACCEPTED MANUSCRIPT

55 R.N. Wenzel, Resistance of Solid Surfaces, Ind. Eng. Chem. 28 (1936) 988-994.

56 Z. Huang, C. Cai, L. Kuai, T. Li, M. Huttula, W. Cao， Leaf-structure patterning for antireflective and self-cleaning surfaces on Si-based solar cells. Solar Energy 159 (2018) 733-741

57 B.Y. Chen, J.H. Qiu, Robust and Superhydrophobic Surface Modification by a "Paint + Adhesive" Method: Applications in Self-Cleaning after Oil Contamination and Oil-Water Separation, ACS Appl. Mater. Interfaces. 27 (2016) 17659-17667.

58 H. Zhou, H. X. Wang, H. T. Niu, A. Gestos, X. G. Wang and T. Lin, Fluoroalkyl silane modified silicone rubber/nanoparticle composite: a super durable, robust superhydrophobic fabric coating, Adv. Mater. 24 (2012) 2409-2412.

59 W. Barthlott, C. Neinhuis, Purity of the sacred lotus, or escape from contamination in biological surfaces, Planta. 202 (1997) 1-8.

60 R. Blossey, Self-cleaning surfaces—virtual realities, Nature Material. 2 (2003) 301-306.

61 R. Furstner, W. Barthlott, C. Neinhuis, P. Walzel, etting and self-cleaning properties of artificial superhydrophobic surfaces, Langmuir. 21 (2005) 956-961.

ACCEPTED MANUSCRIPT

62 D. Quere, Non-sticking drops, Reports on Progress in Physics. 68 (2005) 2495-2532.

63 J.Y. Huang, S.H. Li, M.Z. Ge, L.N. Wang,T.L. Xing,G.Q. Chen, X.F. Liu, S.S. Al-Deyab, K.Q. Zhang, T.Chen and Y.K. Lai, Robust superhydrophobic TiO_2@fabrics for UV shielding, self-cleaning and oil–water separation, J. Mater. Chem. A. 3 (2015) 2825-2832.

64 J. Li, D. Li, Y. Yang, J. Li, F. Zha, Z. Lei, A prewetting induced underwater superoleophobic or underoil (super) hydrophobic waste potato residue-coated mesh for selective efficient oil/water separation. Green. Chem. 18 (2016) 541–549.

65 J. Li, L. Yan, X. Tang, H. Feng, D. Hu, F. Zha, Robust superhydrophobic fabric bag filled with polyurethane sponges used for vacuum-assisted continuous and ultrafast absorption and collection of oils from water, Adv. Mater. Interfaces 3 (2016) 1500770.

66 Y. Long, Y. Shen, H. Tian, Y. Yang, H. Feng, J. Li, Superwettable Coprinus comatus coated membranes used toward the controllable separation of emulsified oil/water mixtures, J. Membr. Sci. 565 (2018) 85–94.

ACCEPTED MANUSCRIPT

67 S.J. Pan, A.K. Kota, J.M. Mabry and A. Tuteja, Superomniphobic surfaces for effective chemical shielding, J. Am. Chem.Soc. 135 (2013) 578-581.

68 S.J. Pan, R. Guo and W.J. Xu, Photoresponsive superhydrophobic surfaces for effective wetting control, Soft Matter. 10 (2014) 9187-9192.

69 S.J. Pan, R. Guo and W.J. Xu, Durable superoleophobic fabric surfaces with counterintuitive superwettability for polar solvents, AIChE J. 60 (2014) 2752-2756.

70 Q.M. Pan, M. Wang, H.B. Wang, Separating small amount of water and hydrophobic solvents by novel superhydrophobic copper meshes, Appl Surf Sci. 254 (2008) 6002-6006.

71 M. Liu, J. Li, L. Shi, Z. Guo, Stable underwater superoleophobic conductive polymer coated meshes for high-efficiency oil–water separation, RSC Adv. 5 (2015) 33077-33082.

72 M. Sun, C. Luo, L. Xu, H. Ji, Q. Ouyang, D. Yu, Y. Chen, Artificial lotus leaf by nanocasting, Langmuir.21 (2015) 8978-8981.

73 W. Meng, Z.j. Feng, F. Li, T.h. Li, W. Cao, Porous coordination polymer coatings fabricated from $Cu_3(BTC)_2 \cdot 3H_2O$ with

ACCEPTED MANUSCRIPT

excellent superhydrophobic and superoleophilic properties, New J. Chem. 40 (2016) 10554.

74 M. Ying, G. Zhang, Sepiolite nanofiber-supported platinum nanoparticle catalysts toward the catalytic oxidation of formaldehyde at ambient temperature: Efficient and stable performance and mechanism, Chem. Eng. J. 288 (2016) 70-78.

75 Y. Gao, H. Gan, G. Zhang, et al, Visible light assisted Fenton-like degradation of rhodamine B and 4-nitrophenol solutions with a stable poly-hydroxyl-iron/sepiolite catalyst, Chem. Eng. J. 217 (2013) 221-230.

ACCEPTED MANUSCRIPT

ACCEPTED MANUSCRIPT

Figure captions

Fig. 1. XRD patterns of sepiolite and $[Ni(2,2'\text{-bipy})_3]Cl_2$ loaded sepiolite. (A) H3 (72 h), (B) H2 (48 h), (C) H1 (24 h), (D) $[Ni(2,2'\text{-bipy})_3]Cl_2$, (E) NaOH treated sepiolite, (F) Sepiolite.

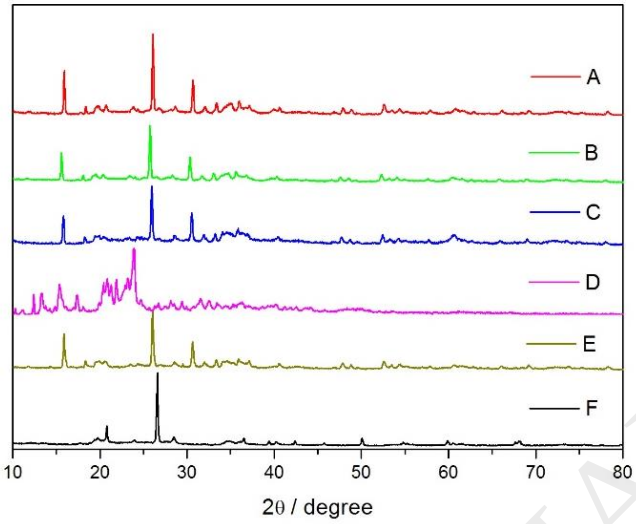

Fig. 2. FT-IR spectra of the as-prepared $[Ni(2,2'\text{-bipy})_3]Cl_2$ /sepiolite catalysts with different hydrothermal reaction time. (A) H3 (72 h), (B) H2 (48 h), (C) H1 (24 h), (D) $[Ni(2,2'\text{-bipy})_3]Cl_2$, (E) NaOH treated sepiolite, (F) Sepiolite.

ACCEPTED MANUSCRIPT

ACCEPTED MANUSCRIPT

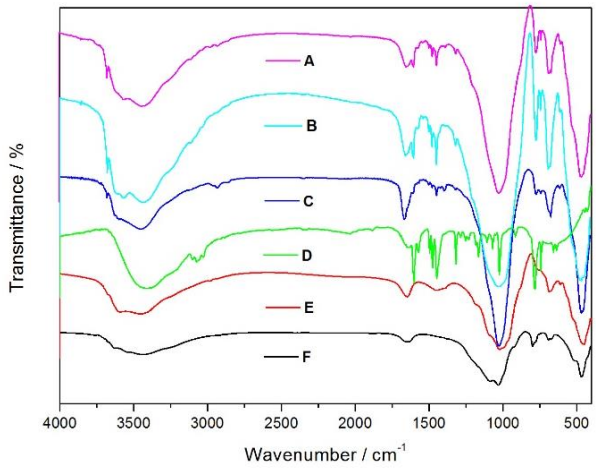

Fig. 3. XPS spectra for the surface of the superhydrophobic [Ni(2,2′-bipy)$_3$]Cl$_2$ /sepiolite catalysts. (A) survey spectrum, (B) C 1s spectra, (C) N 1s spectra, (D) Ni 2p spectra.

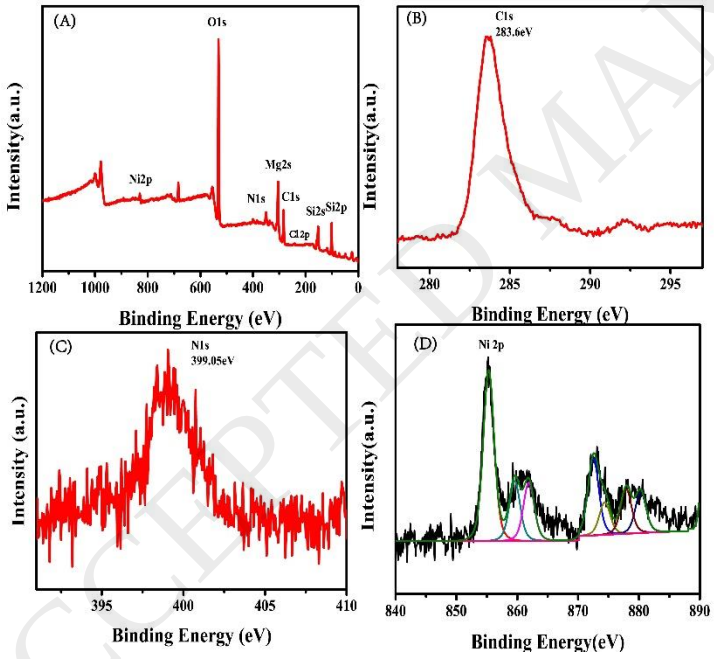

Fig. 4. SEM images of (A) the sepiolite and the as-prepared sample: (B) H1(24 h), (C) H2(48 h) , (D) H3(72 h). TEM (E) and HRTEM (F) images of [Ni(2,2′-bipy)$_3$]Cl$_2$/sepiolite catalysts with hydrothermal reaction time for 48h.

ACCEPTED MANUSCRIPT

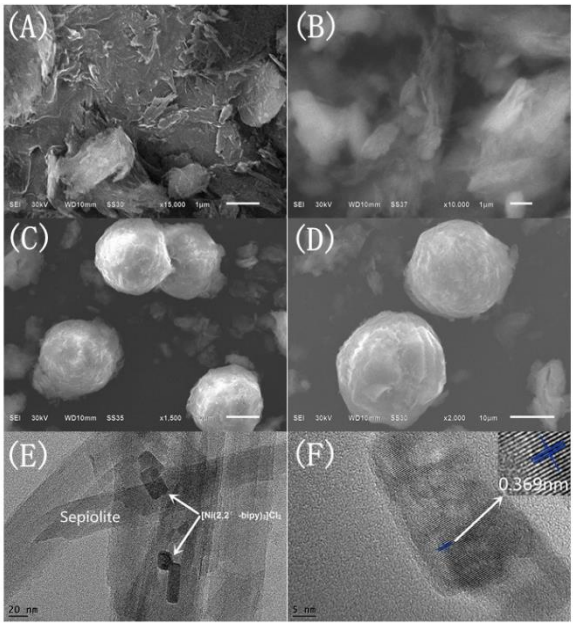

Fig. 5. Photocatalytic degradation results. (A)The photocatalytic degradation rate of RhB under UV-light with different samples. (B)The photocatalytic degradation rate of MO under UV-light with different samples. (C) and (D) Repeated cycles of UV-induced photocatalytic degradation of RhB(A)/MO(B) using the H2 photocatalyst. (E) The photocatalytic hydrogen evolution rate of samples. (F) The stability of H2 under Simulated sunlight irradiation.

ACCEPTED MANUSCRIPT

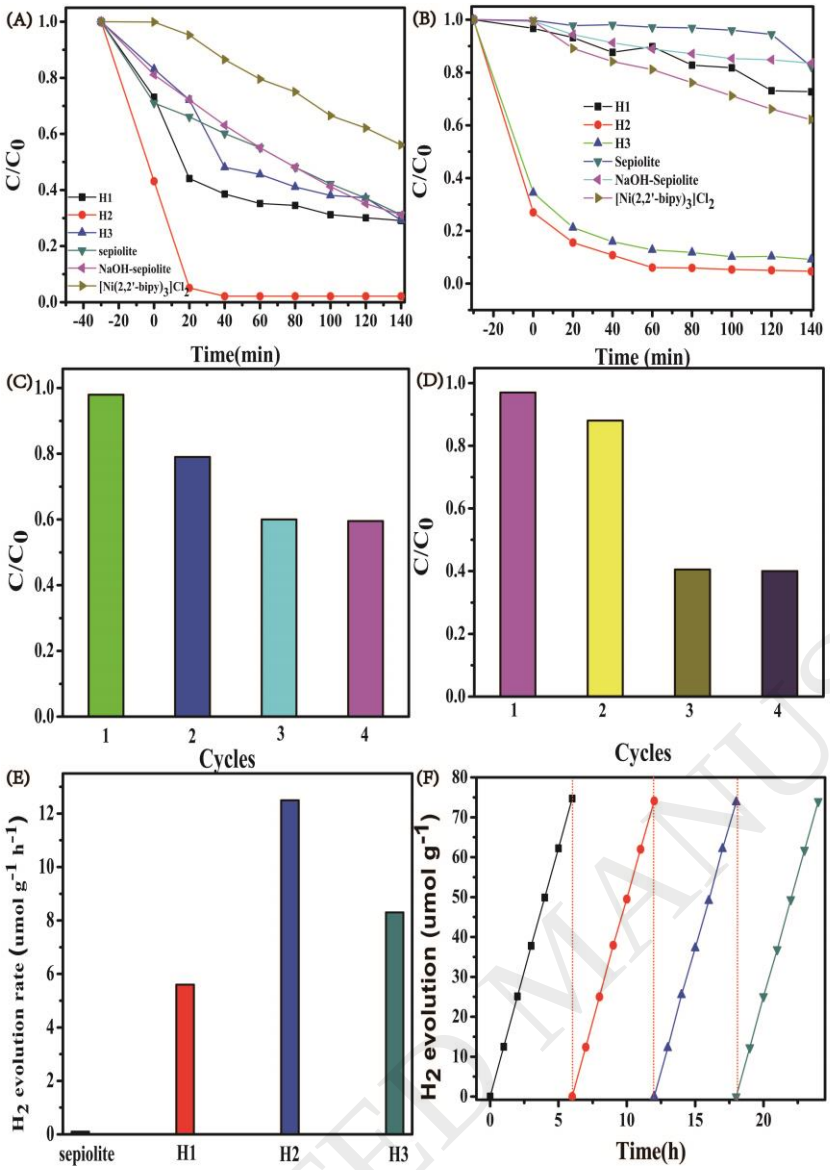

Fig. 6. Time course of the UV-induced photodegradation of RhB using as-prepared nanocatalysts in the presence of various scavengers.

ACCEPTED MANUSCRIPT

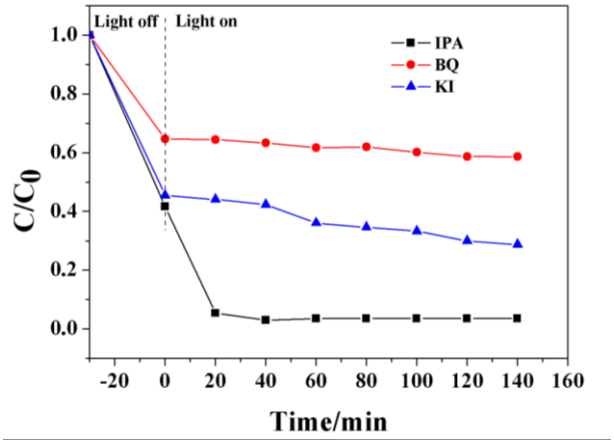

Fig. 7. The photocatalytic mechanism for [Ni (2,2′-bipy)$_3$]Cl$_2$ /sepiolite composite photocatalysts.

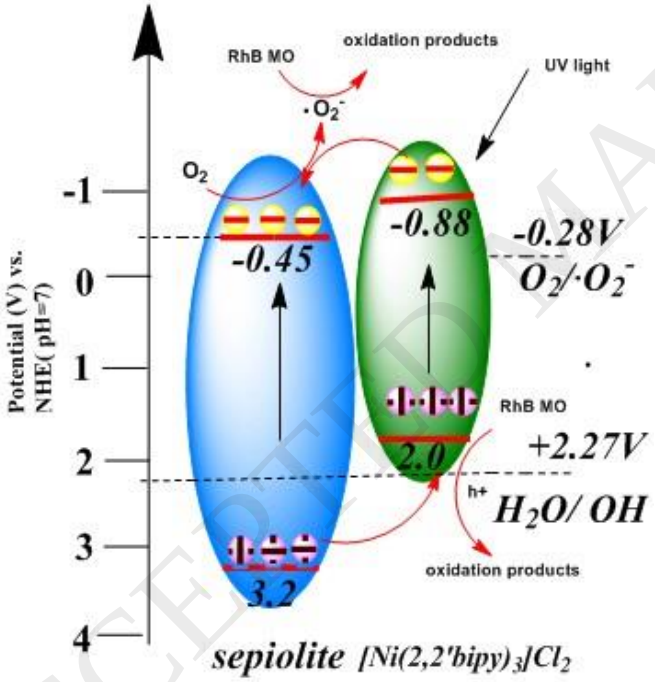

Fig. 8. CAs of water droplets on the surfaces (A) H1(24 h), (B) H2(48 h), (C) H3(72 h) and (D) photo of a water (dyed with methyl bluedroplet) on the film.

ACCEPTED MANUSCRIPT

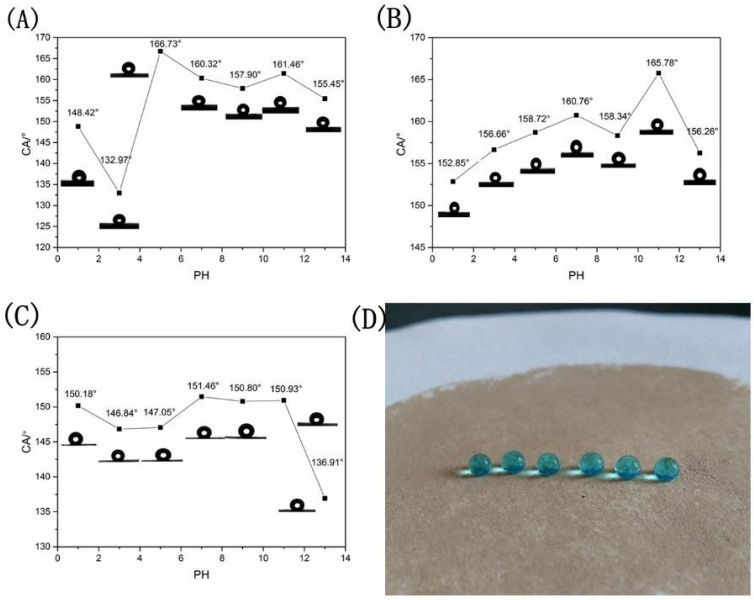

Fig. 9. (A)Water droplets with spherical shape on the tape touched film surface. The inset demonstrated the surface texture of the [Ni(2,2′-bipy)$_3$]Cl$_2$/sepiolite coated fibres (H2,48h) after being scratched for 20 cycles. Demonstration of the superhydrophobicity and knife-scratch tests on the superhydrophobic coating painted surfaces of filter paper. Water droplets can move easily away from the superhydrophobic coating(B-D), and the painted surface retained its water-repellent property even after knife scratches(E-L).

ACCEPTED MANUSCRIPT

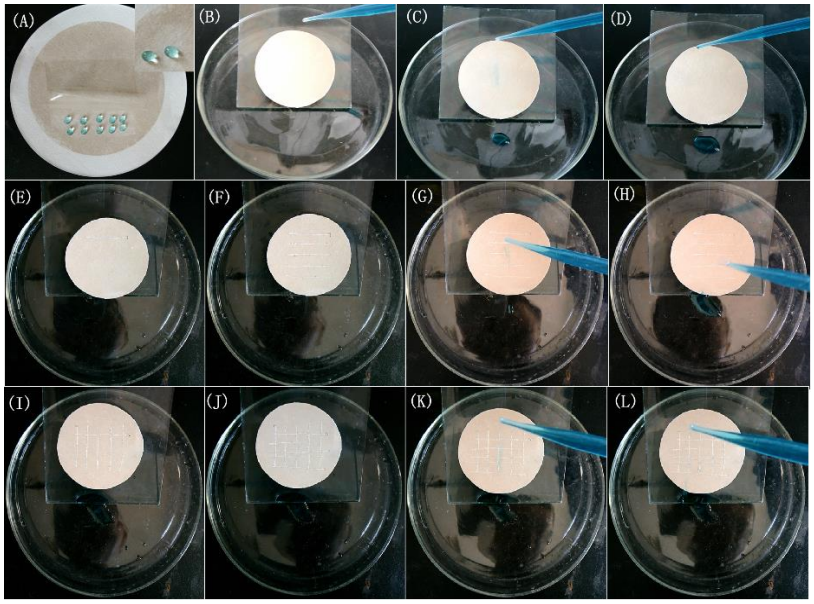

Fig. 10. (A-D) Time sequence of the self-cleaning process on the robust superhydrophobic film with low water adhesion.

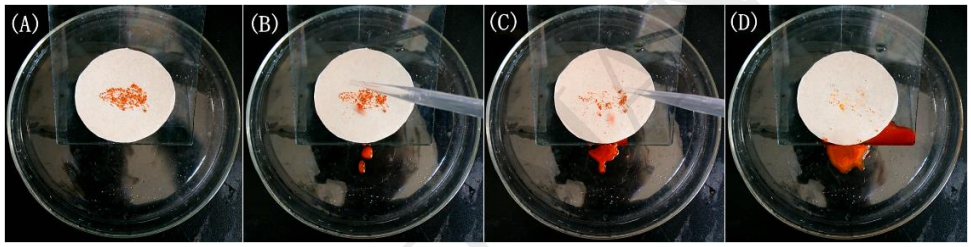

Fig. 11. (A-C) Video snapshots of a drop of octane absorbed by the as-prepared films